Plasmonic Internal Photoemission for Accurate Device In Situ Measurement of Metal-Organic Semiconductor Injection Barriers

*Rijul Dhanker, Neetu Chopra, and Noel C. Giebink**

Current injection in organic semiconductors remains difficult to predict due in large part to the challenge of characterizing the contact energy barrier and interface density of states directly in organic electronic devices. Here, resonant coupling to surface plasmon polariton modes of a metal contact is demonstrated as a means to carry out internal photoemission (IPE) accurately in disordered organic semiconductor devices and enable direct measurement of the contact injection barrier by isolating true IPE from spurious sub-gap organic photoconductivity. The substantial increase in sensitivity afforded by resonant coupling enables measurement in the low-field injection regime where deviation from the standard Fowler prediction is explained quantitatively by the existence of a broad distribution of interface states. This technique is broadly applicable to metals and surface treatments commonly used in organic light emitting diodes, thin film transistors, and photovoltaics, and should therefore provide a quantitative basis to understand and model current injection in these devices over their entire operational lifetime.

1. Introduction

Current injection and extraction at a metal-organic (MO) semiconductor interface is central to the operation of all organic electronic devices, strongly influencing the efficiency of organic light emitting diodes (OLEDs) and photovoltaics as well as the drive current and turn-on voltage of thin film transistors.[1–3] There have been many successful efforts aimed at facilitating injection or engineering carrier selective contact properties,[3,4] however the fundamental physics of injection remains unclear in this class of materials, preventing predictive device design and modeling at the level needed for widespread commercialization. Although MO interfaces are notoriously complex due to, for example, spatially varying disorder,[5] interfacial chemical reactions,[6] and interface roughness,[7] the difficulty in applying and testing present injection models is in large part rooted in the challenge of independently and reliably measuring key parameters such as the injection energy barrier directly in the device geometries in which current–voltage (J–V) characteristics are measured.

Ultraviolet photoelectron spectroscopy (UPS) is arguably the most successful and widely used method for determining energy level alignment at MO interfaces,[8–10] however the energetics deduced from this method as well as its inverse counterpart are not in general the same as that in an actual device due to the difference between surface and bulk polarization energies.[9,10] That is, the energy of a charge carrier near an MO interface is stabilized by polarization and lattice relaxation of the surrounding molecules and the adjacent metal (≈0.5–1 eV), whereas surface-specific techniques such as UPS, Kelvin probe and scanning tunneling microscopy all measure the energy of charge carriers at an organic film surface, stabilized only by polarization from the underlying half-space.

Internal photoemission (IPE) by contrast is carried out directly in the device of interest (i.e., device in situ) and is well established for measuring the injection barrier at metal-inorganic semiconductor contacts.[11,12] In this approach, the metal contact is illuminated directly with visible/near infrared light below the semiconductor bandgap leading to the excitation of hot carriers in the metal. Those carriers with sufficient energy and momenta to surmount the injection barrier, ϕ_B, are emitted into the semiconductor resulting in a photocurrent with yield per absorbed photon, Y, according to the Fowler relationship:[13]

$$Y = A\left(h\nu - \phi_B\right)^2 \quad (1)$$

where A is a constant that reflects the strength of the involved optical transitions. Internal photoemission has previously been applied to MO interfaces,[14,15] however as demonstrated below, interpretation of the data is complicated by the fact that disorder and impurities in organic semiconductors lead to low-level absorption tails extending deep into the optical gap. This sub-gap absorption, together with photo-detrapping transitions within the disorder-broadened highest occupied (HOMO) and lowest unoccupied molecular orbital (LUMO) transport levels leads to a background photocurrent that is difficult to

R. Dhanker, Prof. N. C. Giebink
Department of Electrical Engineering
The Pennsylvania State University
University Park
PA 16802, USA
E-mail: ncg2@psu.edu
Dr. N. Chopra
Plextronics, Inc. 2180 William Pitt Way
Pittsburgh, PA 15238, USA

DOI: 10.1002/adfm.201400344

distinguish from true IPE photocurrent, resulting in the potential for error.

Here, we extend the conventional IPE method by coupling to surface plasmon polariton (SPP) modes[16] of the metal contact to resolve this ambiguity by isolating the IPE signal from background photoconductivity through a fundamental difference in their respective angle-dependent resonance signatures. We apply this approach to the interface between Au and the archetype small molecule hole transport material *N*,*N*′-bis(1-naphthyl)-*N*,*N*′-diphenyl-1,1′-biphenyl-4,4′-diamine (NPD) and find a substantial difference in the barrier heights extracted from conventional and plasmon-coupled IPE at low electric field. Modifying the Fowler relationship to describe IPE into a distribution of states, we show that the plasmon IPE data can be explained by the existence of a broad interface density of states (DOS) that is consistent with the model of injection proposed by Baldo and Forrest.[2] This technique is applicable to a variety of metals in both top and buried contact geometries and therefore should provide a basis for quantitative injection barrier measurement and modeling directly in OLEDs, OPV cells, and OTFTs over their entire operational lifetime.

Figure 1a illustrates the illumination geometry, where a collimated, monochromatic, and transverse-magnetic (TM) polarized beam of light is Kretschmann-coupled[16] to the SPP mode at the cathode/air interface of a typical, sandwich-type device structure consisting of an indium tin oxide (ITO)/organic semiconductor/Au stack. By varying the angle of incidence, the field distribution and thus the power dissipation in each layer of the device changes, as shown by the transfer matrix simulations[17] in Figure 1b. On resonance, nearly all of the incident power can be coupled into the SPP and dissipated in the metal as compared to ≈5% for conventional free space illumination. Assuming that the incoherent hot carrier distribution formed from SPP decay (within ≈100 fs) is the same as that created under nonresonant illumination, this leads to a factor of 10× or more increase in IPE signal to noise ratio.

A more important advantage, however, stems from the fact that power dissipation in the metal peaks on resonance whereas it reaches a minimum in the ITO and organic semiconductor. The angular dependence of the photocurrent thus provides a signature indicating whether IPE from the metal or background organic photoconductivity (or potentially ITO injection) dominates in the measurement: IPE dominates if the photocurrent peaks on resonance whereas spurious photoconductivity (originating from the organic or ITO) dominates if the photocurrent dips on resonance. More generally, by measuring and fitting the reflectivity to a transfer matrix optical model as in Figure 1b, the power dissipation in each layer can be calculated and subsequently used to reconstruct the measured photocurrent in order to quantify what fraction of the photocurrent is due to IPE and what fraction is due to absorption elsewhere in the device.

2. Results and Discussion

To demonstrate this approach, we evaluate the hole injection barrier for an evaporated Au/NPD interface by carrying out both plasmon-coupled and conventional IPE measurements

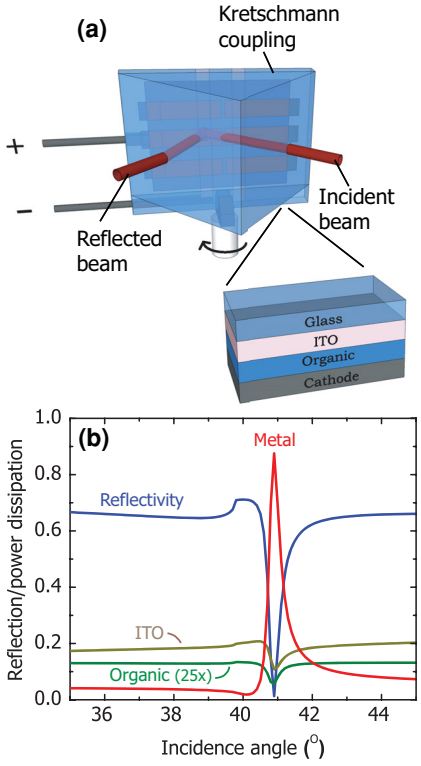

Figure 1. a) Illustration of surface plasmon excitation in a typical thin film device via the Kretschmann configuration together with a schematic of the device structure. b) Reflectivity and power dissipation in each layer of a generic thin film device consisting of ITO (100 nm)/organic semiconductor (100 nm)/Au (40 nm) at $\lambda = 980$ nm predicted using the transfer matrix method. Measured optical constants are used to describe ITO and Au whereas a small extinction coefficient is included for the organic layer ($n = 1.8 + 0.001i$) to model sub-gap absorption. Power dissipation in the metal electrode peaks at 90% on resonance whereas absorption in all other layers of the device reaches a minimum, thereby providing an angular signature from which to distinguish metal versus organic or ITO photocurrent contributions.

on a single layer hole-only device consisting of ITO (100 nm)/NPD (100 nm)/Au (40 nm). The Au/NPD interface was chosen because it is well-characterized by UPS[10] and because NPD has a large optical gap ($E_G = 3.1$ eV) that allows a broad range of visible and near-infrared light to be exploited in the measurement.

Figure 2 displays the reflectivity and photocurrent external quantum efficiency (EQE) measured using synchronous lock-in detection (2 kHz modulation frequency) as a function of incidence angle at four TM-polarized laser wavelengths ($\lambda = 980$, 785, 640, and 543 nm), all of which are well below the nominal absorption edge of NPD ($\lambda > 410$ nm). In each case, the SPP resonance is clearly evident from the dip in reflectivity. Beginning at an excitation wavelength $\lambda = 980$ nm in Figure 2a, we observe that the photocurrent mirrors the SPP reflectivity dip, consistent with the notion that photocurrent originates from power absorbed in the Au and therefore reflects IPE. This is in contrast to the results obtained at $\lambda = 543$ nm in Figure 2d, where the photocurrent dips in unison with the reflectivity, qualitatively indicating that absorption in either the NPD or ITO layer contributes to the photocurrent at this wavelength.

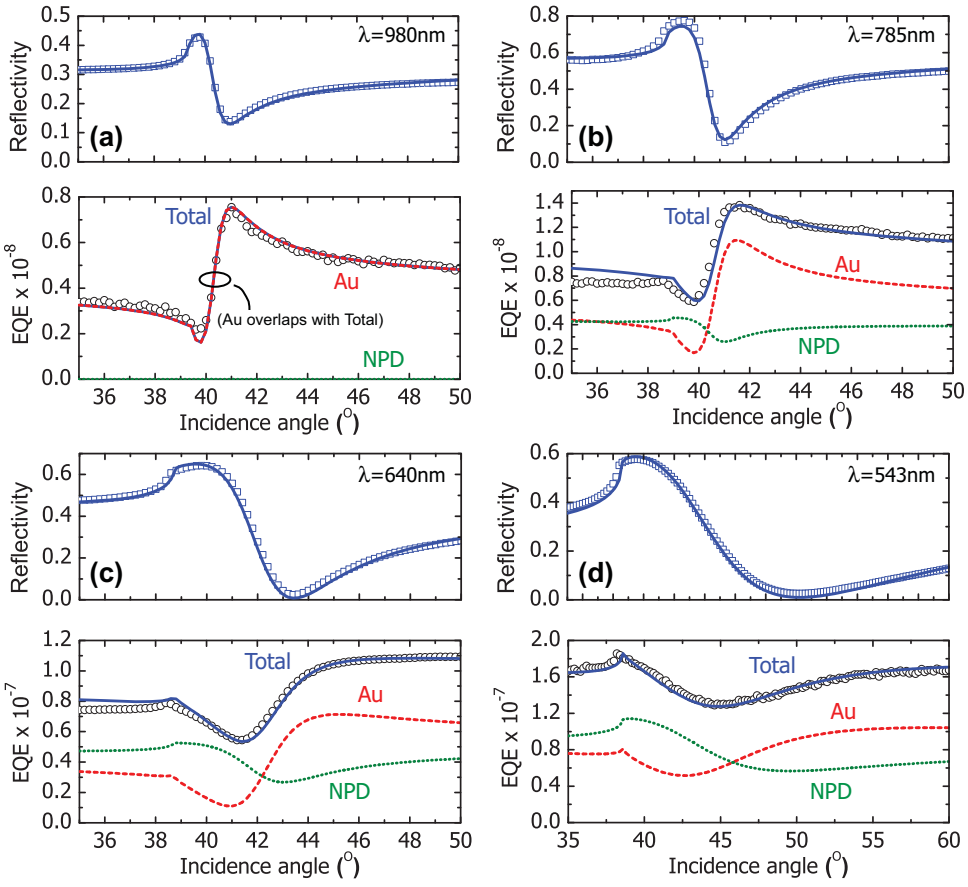

Figure 2. Measured reflectivity and photocurrent external quantum efficiency (EQE) at wavelengths $\lambda = 980$, 785, 640, and 543 nm in sub-figures (a–d). Blue lines indicate fits to the reflectivity and EQE at each wavelength. The fitted component contributions to the EQE from the Au IPE and organic photoconductivity are shown by the red and green dashed lines, respectively. Whereas the EQE is due solely to Au IPE at $\lambda = 980$ nm, there is a substantial contribution from organic photoconductivity at higher photon energies.

The relative contributions of IPE and background photoconductivity to the total EQE are quantified according to a linear superposition based on the fraction of incident power, $\Gamma_i(\theta)$, absorbed in each layer: $\mathrm{EQE} = Y_{\mathrm{Au}}\Gamma_{\mathrm{Au}} + Y_{\mathrm{NPD}}\Gamma_{\mathrm{NPD}} + Y_{\mathrm{ITO}}\Gamma_{\mathrm{ITO}}$. The Γ_i are determined directly from fits to the reflectivity data at each wavelength, leaving the internal quantum yields Y_{Au}, Y_{NPD}, and Y_{ITO} as (constant) fit parameters used in reconstructing the EQE. It is evident from this analysis that nearly half of the photocurrent at $\lambda = 543$ nm (c.f. Figure 2d) does not originate from Au IPE and that this photoconductivity contribution decreases with increasing wavelength. On resonance at the reflectivity minimum, where absorption in the Au maximizes, the IPE-related current fraction is calculated as 62 ± 4%, 69 ± 3%, 80 ± 3%, and 100% at wavelengths of $\lambda = 543$, $\lambda = 640$, $\lambda = 785$, and $\lambda = 980$ nm, respectively. This trend is qualitatively consistent with the existence of tail-state absorption decaying deep into the NPD optical gap[18] although we cannot definitively rule out a contribution from ITO due the functional similarity between Γ_{NPD} and Γ_{ITO}.

Figure 3 confirms that the photocurrent is a superposition of different physical sources by comparing the modulation frequency dependence of the EQE magnitude on and off ($\theta_{\mathrm{off}} = 35°$) the SPP angular resonance. For $\lambda = 980$ nm excitation (Figure 3a), the frequency response on and off resonance is nearly identical, consistent with the sole contribution from Au identified in Figure 2a. By contrast, there is a substantial difference for $\lambda = 640$ nm excitation (Figure 3b), indicating that the relative photocurrent contributions on and off resonance differ as predicted in Figure 2c.

The deconvolved plasmon IPE yields on resonance are plotted in **Figure 4**b according to Equation 1 for different bias levels (Au positive) set to probe hole injection from Au into NPD. These data are compared with conventional IPE measurements of the same device in Figure 4a, which were carried out using a monochromated Xe lamp incident from air onto the Au electrode at an angle $\theta \approx 15°$. Both the plasmon and conventional IPE follow an approximately linear dependence, which is perhaps surprising in the latter case given the substantial NPD photocurrent contribution presumed in the 1.5–2.0 eV photon energy range. This unfortunate coincidence, wherein conventional IPE data follows the Fowler relationship despite substantial non-IPE current contributions, may be a general problem for disordered semiconductors since Taylor expanding the exponentially decaying tail state absorption coefficient in energy inevitably leads to quadratic terms that mimic the Fowler prediction.

Consequently, it is not often possible to identify the existence of artifact photoconductivity let alone discern its contribution

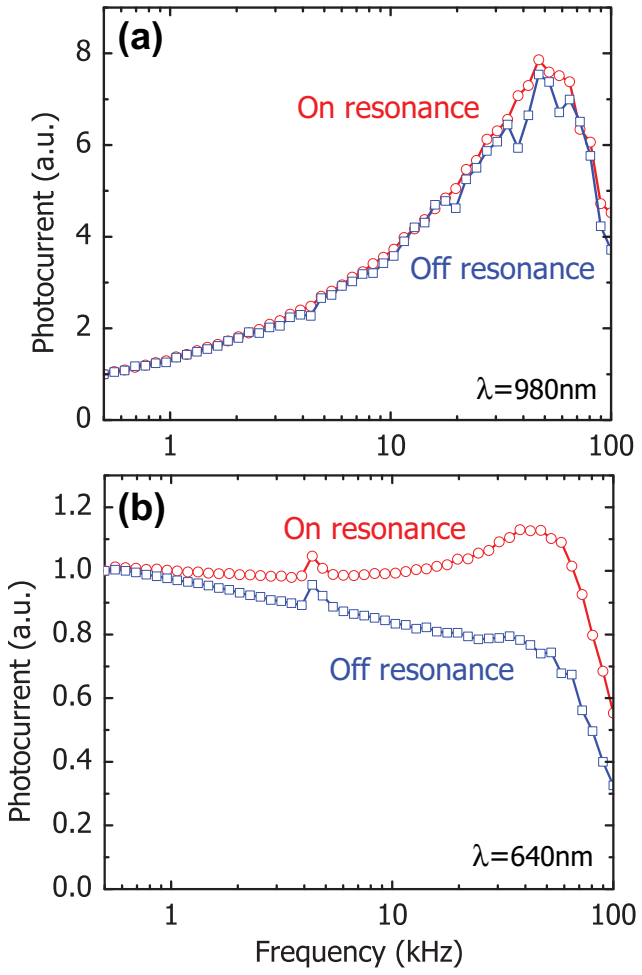

Figure 3. Dependence of the normalized photocurrent magnitude on laser modulation frequency obtained on and off the surface plasmon resonance angle for a) $\lambda = 980$ nm and b) $\lambda = 640$ nm. The difference in the trends at $\lambda = 640$ nm indicates that there are different sources of photocurrent that dominate on and off resonance as calculated in Figure 2. Measurement at $\lambda = 785$ nm (not shown) displayed an on/off difference in frequency response intermediate to that shown in (a,b).

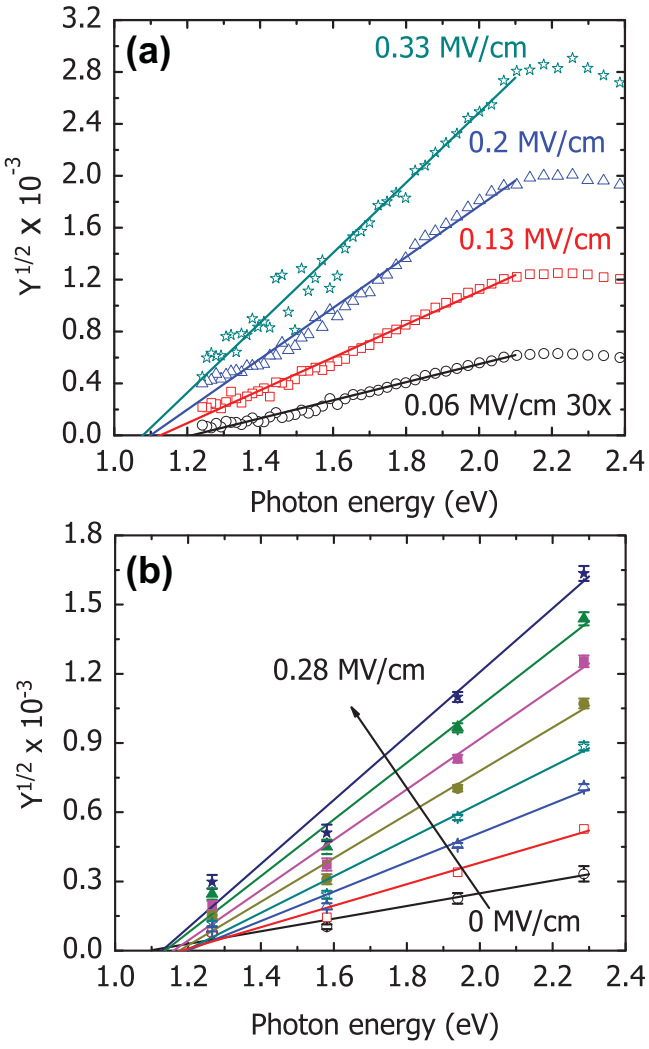

Figure 4. Fowler plot for a) conventional and b) plasmon-deconvolved internal photoemission data for different applied electric fields in the device. The devices are fully depleted over the investigated bias range and the internal electric field was measured using electroabsorption. The increased sensitivity afforded by of plasmon coupling enables internal photoemission signal even at zero applied field as discussed in the text.

in conventional IPE applied to organic semiconductor thin films. It is notable that the photoconductivity observed here persists below half of the 3.1 eV NPD optical gap, implying that this issue may pose an even greater problem in narrower gap materials. Since the magnitude of the injection barrier sets a lower limit on the photon energy used to generate IPE, a photoconductivity contribution may be unavoidable in these cases, making the distinction provided by SPP coupling key to an accurate measurement.

Barrier energies (ϕ_B) corresponding to the abscissa intercepts[19] in Figure 4 are summarized in **Figure 5** as a function of electric field, F, according to the standard image force lowering relationship $\phi_B(F) = \phi_{B0} - K\sqrt{F}$. Here, ϕ_{B0}, is the zero-field barrier, K is the field-dependent lowering coefficient and the applied field F is constant throughout the device according to capacitance–voltage (CV) measurements that indicate depletion of mobile charge [i.e., C(V) is constant and equal to the geometric capacitance] over the investigated bias range. To accurately obtain the internal electric field in the device, the built-in potential (V_{bi}) is measured via electroabsorption[15] and found to be zero within experimental error.

Whereas the plasmon-coupled and conventional IPE barriers are in reasonable agreement at high fields, the low-field functional dependence of the plasmon data differs markedly from the straight line expectation of the image force lowering relationship. From a data analysis standpoint, this reflects a larger-than-expected plasmon IPE current at low photon energies that pushes the fit intercept to lower energy. We propose that this deviation is due to energetic disorder at the interface that leads to a distribution of injection barriers. This hypothesis is supported by observation of clear plasmon IPE for $\lambda = 1550$ nm excitation (0.8 eV photon energy) in **Figure 6**a, which is well below the zero-field barrier extrapolated from the conventional ($\phi_{B0} = 1.30 \pm 0.05$ eV) or high-field plasmon IPE

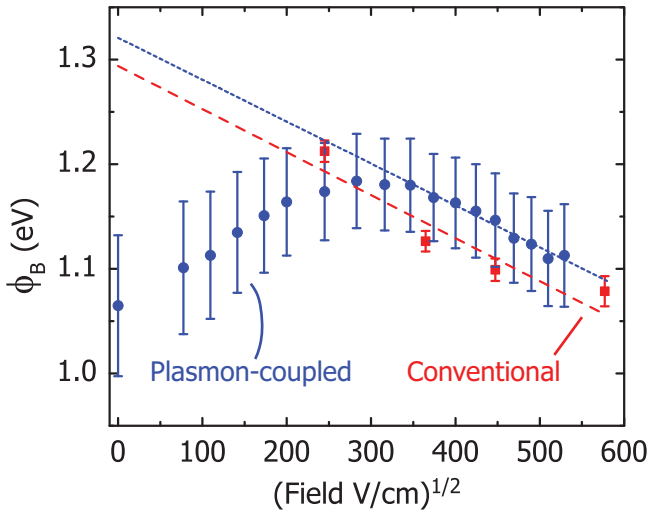

Figure 5. Injection barriers extracted from plasmon-coupled and conventional IPE as a function of internal electric field in the device. Whereas linearity at high fields is consistent with image force barrier lowering, deviation in the plasmon data at low fields is suggested to reflect an increasing contribution from low energy injection barriers that originate from a broad density of states distribution at the interface. Error bars for the plasmon data are large due to the limited number of laser wavelengths available for measurement in Figure 4b.

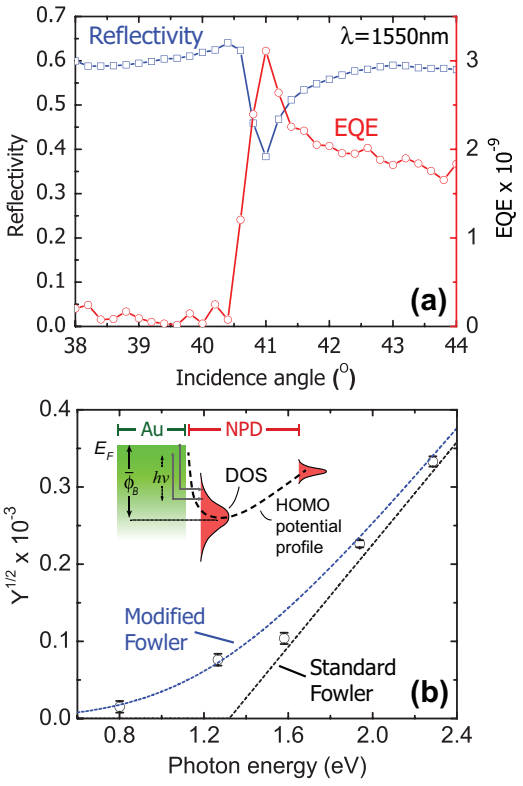

Figure 6. a) Reflectivity and photocurrent measured at zero applied electric field and $\lambda = 1550$ nm (0.8 eV), significantly below the barrier ϕ_{B0} extrapolated from Figure 5, suggesting a distribution of electronic states at the Au/NPD interface as depicted in the inset diagram of (b). There, a revised Fowler plot including the low energy $\lambda = 1550$ nm data is modeled by assuming injection into a Gaussian distribution of states with a mean barrier height $\bar{\phi}_{B0} = 1.32$ eV and broadening $\sigma = 350$ meV. The prediction of the standard Fowler model ($\sigma = 0$) is labeled and shown for comparison.

($\phi_{B0} = 1.32 \pm 0.09$ eV) data. This zero-field result is consistent with the 1.4 eV barrier height measured via UPS for NPD deposited on pristine Au,[20] but is lower because it includes the full bulk (as opposed to only the surface) polarization of the organic as discussed above.

The nominally "sub-barrier" IPE at λ = 1550 nm can be understood on the basis of interface energetic disorder by assuming an approximately Gaussian distribution of injection barrier heights, $g(\phi_B) = \left[1/\sigma\sqrt{2\pi}\right]\exp\left[-(\phi_B - \bar{\phi}_B)^2/2\sigma^2\right]$, with half-width σ and mean barrier height $\bar{\phi}_B$. Integrating the Fowler equation over this distribution from the metal Fermi energy (0 eV) to the incident photon energy ($h\nu$) under the assumption that $\sigma \ll \bar{\phi}_B$ yields a finite IPE yield $Y \approx A\sigma^2/2$ when $h\nu = \bar{\phi}_B$ instead of the zero intercept expected from Equation 1. Figure 6b re-plots the zero field data from Figure 4a including the $\lambda = 1550$ nm point and compares it to a numerical evaluation of the disorder-modified Fowler relationship. Fixing $\bar{\phi}_{B0} = 1.32$ eV from the high-field extrapolation from Figure 5, we find that σ = 350 meV enables much closer agreement with the data, exhibiting a "soft" cutoff that asymptotes toward zero at low photon energy due to the lower energy states (i.e., injection barriers) in the distribution. This distribution width is similar in magnitude to that calculated by Baldo and Forrest,[2] who predicted that injection at MO interfaces is dominated by hopping through an interface DOS substantially broader than that in the bulk.

The apparent manifestation of energetic disorder in low-field IPE data can be understood to first order from the location of the field-lowered image potential maximum relative to the electrode interface. At high field, the maximum occurs close to the electrode (<1 nm) enabling IPE access to the majority of the DOS whereas at low field the maximum occurs farther away (>3 nm beyond the range of the initial injection event)[21] and thus injection in the DOS tail becomes a comparatively more significant pathway for IPE current. The low-field regime (<10^5 V cm^{-1}) is not usually accessed in conventional IPE experiments[14,15] owing to low signal and thus the sensitivity boost enabled by plasmon coupling may open up a unique opportunity to probe the interface DOS distribution.

To this final point, it is notable that plasmon IPE current is clearly evident at short circuit despite the nominally zero internal electric field (c.f. Figure 4b). Indeed, we find that a voltage of approximately 0.35 V is required to null the plasmon IPE current (i.e., where the photocurrent magnitude nulls and the phase changes by 180 degrees) under $\lambda = 980$ nm illumination, increasing to 0.6 V at $\lambda = 543$ nm, independent of intensity. This effect has been observed and described before in terms of the imbalance of IPE current between electrodes, where for one-sided plasmon injection, the maximum voltage is given by $V_{oc} = (h\nu - \phi_B)/q$.[22] This equation, however, is derived for very thin insulating barriers <5 nm assuming ballistic transport from one contact to the other, invalid for the case at hand. It is not yet clear to what extent this relationship still holds when injection is followed by drift/diffusion in the bulk, as our voltage data scale nonlinearly with photon energy. The very existence of an IPE null voltage for such a thick organic film

is nonetheless somewhat surprising and may yield additional insight into the interface energetics with the development of a rigorous theoretical treatment.

3. Conclusion

In summary, we have demonstrated surface plasmon-coupled IPE as a method to obtain accurate photoemission yields in disordered organic semiconductor thin film devices. In comparison with conventional IPE measurements carried out on the same devices, the increased sensitivity of plasmon coupling combined with the capability to reject spurious contributions from sub-gap tail state photoconductivity led to a substantial difference in extracted barrier heights at low field. A model based on interface energetic disorder was proposed to explain this result, enabling both the mean barrier height and its disorder width to be estimated using plasmon-coupled IPE measurements. Moving forward, it will be important to extend this technique over a wider and denser wavelength range in order to more rigorously explore the validity of this hypothesis.

In this context, plasmon-coupled IPE should be a broadly applicable tool since many of the metals used in organic electronic devices directly support SPP modes (e.g., Au, Ag, Al, Ni, Cu)[23] or are included in compound contacts (e.g., Mg/Ag, MoO_3/Au)[2,24] with SPPs supported by the capping metal. Whereas top contact injection barriers are easily probed via prism-coupling as demonstrated here, applying this technique to probe buried contacts would require an underlying grating to supply the larger momentum mismatch between free space and the metal/organic interface SPP modes.

More generally, the efficiency of SPP photoinjection also opens up new opportunities for transient characterization, such as time-of-flight mobility directly in OLED and OPV-relevant film thicknesses because it creates a highly localized carrier population in both space and time. By coupling accurate IPE and bulk mobility measurements together with current-voltage data obtained in the same device, this approach opens up an important opportunity to test theoretical injection models with more rigor and confidence to progress toward a unified description of injection in organic semiconductors.

4. Experimental Section

Sample Preparation: Devices were fabricated on solvent cleaned, pre-patterned ITO coated glass (100 nm thick, sheet resistance 20 Ω/square). The substrates were subsequently treated with air plasma for 5 minutes and then immediately loaded into a thermal evaporation chamber (base pressure 10^{-7} Torr) for deposition of NPD at a rate of 3 Å s^{-1}. Contacts were defined using a shadow mask in a N_2 filled glove box followed by evaporation of 40 nm of Au at 1 Å s^{-1} to yield active device areas of 4×10^{-2} cm^2.

IPE Measurements: Reflectivity and EQE measurements for plasmon-coupled IPE were carried out using a pair of computer-controlled rotation stages using four diode lasers (λ = 640, 785, 980, 1550 nm) and a green HeNe laser (λ = 543 nm). Transverse magnetic polarization was used in all cases and the lasers were modulated directly (diodes) or chopped mechanically (HeNe) for synchronous photocurrent detection using a low noise current preamplifier (SR570, Stanford Research Systems) and a lock-in amplifier (SR830). Conventional IPE measurements were carried out using monochromated light from a Xe lamp (LDLS EQ-99, Energetiq) incident directly on the Au contacts at an angle of approximately 15°, maintaining the same photocurrent detection system. Use of the monochromated Xe lamp for plasmon-coupled IPE measurements was precluded by brightness considerations: plasmon coupling requires highly collimated light to resolve the angular photocurrent dependence whereas high numerical aperture collection was required to gather sufficient power from the lamp to measure the low-level IPE current.

IPE Analysis: Angular EQE data were deconvolved by first fitting the associated reflectivity profiles using the transfer matrix method together with optical constants from each layer measured by variable angle spectroscopic ellipsometry. Because ellipsometry is not sensitive to low level absorption, we do not know the sub-gap extinction coefficient of NPD precisely. However, because the sub-gap NPD extinction is small, it has negligible impact on the functional form of the power dissipation angular profile and so we simply fix it at $k = 10^{-3}$, leaving the magnitude of Γ_{NPD} to be lumped in with the fitted NPD photocurrent yield, Y_{NPD}. Due to the functional similarity between Γ_{NPD} and Γ_{ITO}, it is not possible to distinguish between NPD and ITO photocurrent (i.e., Y_{NPD} and Y_{ITO} are correlated in any fit). We thus set $Y_{ITO} = 0$, using only Y_{NPD} and Y_{Au} to fit the photocurrent profiles in Figure 2 and acknowledge that some component of the nominal NPD contribution may arise from ITO. Accounting for the decrease in hot electron attenuation length with increasing photon energy[11,25] was found to be important for enabling accurate photocurrent reconstruction. This effect was included to first order in the model by calculating Y_{Au} using only the power dissipated within a given distance, x_d, of the organic interface. This distance impacts the functional form of the Y_{Au} angular dependence and is readily evident when reconstructing the photocurrent. The values used for the reconstructions of Figure 2 are x_d = 40, 31, 27, and 20 nm for λ = 980, 785, 640, and 543 nm, respectively, in good agreement with previous measurement.[26]

Acknowledgements

This work was supported in part by the Dow Chemical Company as part of the Flexible Electronics initiative. The authors also thank Dr. Jerzy Ruzyllo for use of the impedance analyzer and Dr. Susan Trolier-McKinstry for use of the variable angle spectroscopic ellipsometer.

Received: January 31, 2014
Revised: March 20, 2014
Published online: May 3, 2014

[1] a) G. G. Malliaras, C. J. Scott, *J. Appl. Phys.* **1998**, *83*, 5399; b) Y. L. Shen, M. W. Klein, D. B. Jacobs, J. C. Scott, G. G. Malliaras, *Phys. Rev. Lett.* **2001**, *86*, 3867; c) D. J. Gundlach, L. L. Jia, T. N. Jackson, *IEEE Electron Dev. Lett.* **2001**, *22*, 571; d) J. C. Scott, *J. Vac. Sci. Technol. A* **2003**, *21*, 521.
[2] M. A. Baldo, S. R. Forrest, *Phys. Rev. B* **2001**, *64*, 085201.
[3] Y. Zhou, C. Fuentes-Hernandez, J. Shim, J. Meyer, A. J. Giordano, H. Li, P. Winget, T. Papadopoulos, H. Cheun, J. Kim, M. Fenoll, A. Dindar, W. Haske, E. Najafabadi, T. M. Khan, H. Sojoudi, S. Barlow, S. Graham, J. L. Bredas, S. R. Marder, A. Kahn, B. Kippelen, *Science* **2012**, *336*, 327.
[4] M. D. Irwin, B. Buchholz, A. W. Hains, R. P. H. Chang, T. J. Marks, *Proc. Natl. Acad. Sci.* **2008**, *105*, 2783.
[5] a) N. Tessler, Y. Preezant, N. Rappaport, Y. Roichman, *Adv. Mater.* **2009**, *21*, 2741; b) S. V. Novikov, G. G. Malliaras, *Phys. Rev. B* **2006**, *73*, 033308.
[6] a) P. Dannetun, M. Lögdlund, M. Fahlman, M. Boman, S. Stafström, W. R. Salaneck, R. Lazzaroni, C. Fredriksson, J. L. Brédas, S. Grahm, R. H. Friend, A. B. Holmes, R. Zamboni,

C. Taliani, *Synth. Met.* **1993**, *55*, 212; b) P. Dannetun, M. Fahlman, C. Fauquet, K. Kaerijama, Y. Sonoda, R. Lazzaroni, J. L. Brédas, W. R. Salaneck, *Synth. Met.* **1994**, *67*, 133; c) M. Fahlman, D. Beljonne, M. Lögdlund, R. H. Friend, A. B. Holmes, J. L. Brédas, W. R. Salaneck, *Chem. Phys. Lett.* **1993**, *214*, 327.

[7] B. N. Limketkai, M. A. Baldo, *Phys. Rev. B* **2005**, *71*, 085207.

[8] H. Ishii, K. Sugiyama, D. Yoshimura, E. Ito, Y. Ouchi, K. Seki, *IEEE J. Sel. Top. Quant.* **1998**, *4*, 24.

[9] S. Braun, W. R. Salaneck, M. Fahlman, *Adv. Mater.* **2009**, *21*, 1450.

[10] J. Hwang, A. Wan, A. Kahn, *Mater. Sci. Eng. Rep.* **2009**, *64*, 1.

[11] C. R. Crowell, L. E. Howarth, W. G. Spitzer, E. E. Labate, *Phys. Rev.* **1962**, *127*, 2006.

[12] a) C. N. Berglund, W. E. Spicer, *Phys. Rev. A* **1964**, *136*, 1044; b) B. E. Deal, E. H. Snow, C. A. Mead, *J. Phys. Chem. Solids* **1966**, *27*, 1873.

[13] R. H. Fowler, *Phys. Rev.* **1931**, *38*, 45.

[14] a) G. Rikken, D. Braun, E. G. J. Staring, R. Demandt, *Appl. Phys. Lett.* **1994**, *65*, 219; b) I. H. Campbell, D. L. Smith, *Appl. Phys. Lett.* **1999**, *74*, 561; c) P. Sigaud, J. N. Chazalviel, F. Ozanam, O. Stephan, *J. Appl. Phys.* **2001**, *89*, 466; d) H. J. Gaehrs, F. Willig, *Chem. Phys. Lett.* **1975**, *32*, 300.

[15] I. H. Campbell, T. W. Hagler, D. L. Smith, J. P. Ferraris, *Phys. Rev. Lett.* **1996**, *76*, 1900.

[16] H. Raether, *Surface plasmons on smooth and rough surfaces.*, Springer, New York, NY **1988**.

[17] P. Yeh, *Optical waves in layered media.*, Wiley, Hoboken, NJ **2005**.

[18] a) M. Stella, C. Voz, J. Puigdollers, F. Rojas, A. Fonrodona, J. Escarre, J. M. Asensi, J. Bertomeu, J. Andreu, *J. Non-Cryst. Solids* **2006**, *352*, 1663; b) L. Goris, K. Haenen, M. Nesladek, A. Poruba, M. Vanecek, P. Wagner, L. Lutsen, J. V. Manca, D. Vanderzande, L. De Schepper, *Organ. Optoelectron. Photonics* **2004**, *5464*, 372.

[19] S. M. Sze, *Physics of semiconductor devices.*, Wiley, New York, NY **2005**.

[20] a) N. Koch, A. Kahn, J. Ghijsen, J.-J. Pireaux, J. Schwartz, R. L. Johnson, A. Elschner, *Appl. Phys. Lett.* **2003**, *82*, 70; b) A. Wan, J. Hwang, F. Amy, A. Kahn, *Org. Electron.* **2005**, *6*, 47.

[21] V. I. Arkhipov, U. Wolf, H. Bassler, *Phys. Rev. B* **1999**, *59*, 7514.

[22] a) F. M. Wang, N. A. Melosh, *Nano Lett.* **2011**, *11*, 5426; b) F. M. Wang, N. A. Melosh, *Nature Comm.* **2013**, *4*, 1711.

[23] a) J. C. Quail, J. G. Rako, H. J. Simon, *Opt. Lett.* **1983**, *8*, 377; M. Weisenberg, K. Aslan, E. Hortle, C. D. Geddes, *Chem. Phys. Lett.* **2009**, *473*, 120; d) M. J. R. Previte, Y. Zhang, K. Aslan, C. D. Geddes, *Appl. Phys. Lett.* **2007**, *91*, 151902.

[24] C. W. Chu, S. H. Li, C. W. Chen, V. Shrotriya, Y. Yang, *Appl. Phys. Lett.* **2005**, *87*, 193508.

[25] P. A. Wolff, *Phys. Rev.* **1954**, *95*, 56.

[26] R. W. Soshea, R. C. Lucas, *Phys. Rev.* **1965**, *138*, 1182.